Downslope Flows on a Low-Angle Slope and Their Interactions with Valley Inversions. Part I: Observations

C. DAVID WHITEMAN*

Department of Meteorology, University of Utah, Salt Lake City, Utah

SHIYUAN ZHONG

Department of Geography, Michigan State University, East Lansing, Michigan

(Manuscript received 18 December 2006, in final form 12 December 2007)

ABSTRACT

Thermally driven downslope flows were investigated on a low-angle (1.6°) slope on the west side of the floor of Utah's Salt Lake Valley below the Oquirrh Mountains using data from a line of four tethered balloons running down the topographic gradient and separated by about 1 km. The study focused on the evolution of the temperature and wind structure within and above the slope flow layer and its variation with downslope distance. In a typical situation, on clear, undisturbed October nights a 25-m-deep temperature deficit of 7°C and a 100–150-m-deep downslope flow with a jet maximum speed of 5–6 m s^{-1} at 10–15 m AGL developed over the slope during the first 2 h following sunset. The jet maximum speed and the downslope volume flux increased with downslope distance. The downslope flows weakened in the late evening as the stronger down-valley flows expanded to take up more of the valley atmosphere and as ambient stability increased in the lower valley with the buildup of a nocturnal temperature inversion. Downslope flows over this low-angle slope were deeper and stronger than has been reported previously by other investigators, who generally investigated steeper slopes and, in many cases, slopes on the sidewalls of isolated mountains where the downslope flows are not subject to the influence of nighttime buildup of ambient stability within valleys.

1. Introduction

Thermally driven downslope flows are observed in mountain ranges throughout the world. They typically form in the late afternoon or evening when the sensible heat flux over a slope becomes negative and a temperature deficit develops above the slope relative to the air at the same elevation away from the slope. These flows are a type of katabatic flow—a general term that also includes other thermally driven flows such as down-valley flows, combinations of downslope and down-valley winds, and, even, continental-scale drainage flows over the ice dome of Antarctica (Poulos 1997). Downslope flows have been extensively observed and modeled. Nonetheless, specialized downslope-flow datasets have been largely unavailable to answer key scientific questions about the downslope flows for the typical ranges of internal (slope angle, roughness, sensible heat flux, and radiative flux divergence) and external (winds above the slope layer and ambient stability) parameters. A proliferation of analytical and numerical models has not been matched by observations, with the result that some important questions about slope flows are still unresolved, and it is difficult to identify suitable models for different circumstances.

Much experimental effort in the past has been focused on flows on two-dimensional slopes on the sides of isolated mountains (termed "simple slopes" in the literature) where three-dimensional topographic effects, diurnal changes in ambient stability, and the influence of overriding along-valley flows are minimized. A general finding for such flows is that the depth of the downslope flow increases with distance down the slope to maintain a depth that is about 5% of the elevation

* Certified Consulting Meteorologist (CCM)

Corresponding author address: C. David Whiteman, CCM, Department of Meteorology, University of Utah, 135 S 1460 E, Rm. 819, Salt Lake City, UT 84112-0110.
E-mail: dave.whiteman@utah.edu

DOI: 10.1175/2007JAMC1669.1

drop to the measurement point (Briggs 1979; Horst and Doran 1986). Current mesoscale numerical models are known generally to overpredict the depth and strength of both upslope and downslope flows (J. D. Fast 2002, personal communication). Because of computer and model limitations, the vertical resolution in simulations of valley- or basin-sized volumes has been generally insufficient to depict accurately the shallow slope flows and their role in driving the valley circulations. Observations and model limitations have led to uncertainties about the relative roles of radiative and turbulent sensible heat flux divergence in driving the flows, and there are wide discrepancies among models in very basic characteristics of the slope flows, including, for example, whether downslope flows are stronger on steep or shallow slopes. Because many of the previous slope-flow experiments have been conducted on the sides of isolated mountains rather than on the sidewalls of valleys, the effects of the normal nocturnal buildup of temperature inversions in valleys on downslope flows has not been adequately studied.

The dearth of observational studies on valley sidewalls is caused by a number of observational difficulties. Valley sidewalls are usually very nonideal sloping surfaces, containing numerous small-scale terrain, vegetation, and soil features. Because the downslope airflow near the ground responds readily to these features, it is difficult to choose representative measurement locations on slopes. Further complications include the sensitivity of the downslope flows to winds above the slope-flow layer (especially the along-valley winds that develop under the same conditions as the slope flows), the difficulty of measuring and interpreting sensible heat and radiative fluxes on sloping surfaces, and the problems of choosing and installing instrumentation to gain appropriate vertical resolution through the full depth of the slope flows. The inhomogeneity and nonstationarity of the downslope flows also present a challenge to field experiments.

This paper uses data collected from a line of four tethered balloons running down the slope and separated by about 1 km each to investigate thermally driven downslope flows that develop on clear, undisturbed nights on a low-angle slope in the Salt Lake Valley of Utah that is near ideal topographically. It describes the experimental design, the location of the experiments, the equipment used, and the datasets collected. Initial analyses of the structure and evolution of the flows are provided, including the development of atmospheric structure with downslope distance and the relationship of the structural changes to the growth of a nighttime temperature inversion within the valley. Because the datasets provide new information on downslope flows that develop on low-angle slopes deep within valleys where the ambient temperature structure undergoes regular diurnal changes, the data should prove useful for the future testing of conceptual, analytical, and numerical slope-flow models. A companion paper (Zhong and Whiteman 2008, hereinafter Part II) applies a full-physics numerical model to simulate the slope-flow observations reported in this paper and investigates further the relationship between slope flows and ambient stability, cross-slope flow, and roughness length. A paper by Haiden and Whiteman (2005) used these data to assess the individual terms of the slope-flow momentum and heat balances using a variety of analytical katabatic flow models. Skyllingstad (2003) and Smith and Skyllingstad (2005) used a large-eddy simulation model to simulate the observed downslope flows.

2. The slope experiment

a. Experiment design

The slope-flow experiment was conducted as part of an intensive field campaign, the Vertical Transport and Mixing (VTMX) experiment, which was sponsored by the U.S. Department of Energy and took place in October of 2000 in the Salt Lake Valley.[1] The goal of VTMX was to investigate the physical processes that affect vertical transport and mixing in urban valley environments. An overview of the VTMX experiments was published by Doran et al. (2002), and research in VTMX has focused on intermittent turbulence (Doran 2004; Monti et al. 2002), elevated stratified layers (Coulter et al. 2004), air-motion tracer dispersal (Fast et al. 2006; Allwine et al. 2002), and canyon and gap flows (Banta et al. 2004; Pinto et al. 2006). Because slope flows play an important role in horizontal and vertical transport in valleys, we designed and executed a set of slope-flow experiments that were run as part of VTMX. The objectives of the slope-flow experiments were to investigate 1) the characteristics and temporal evolution of the downslope flows, 2) the development of the downslope flows with downslope distance, 3) the dependence of downslope-flow characteristics on ambient stability, and 4) the sensitivity of the downslope flows to overlying along-valley and synoptic flows.

[1] The "Salt Lake Valley," in popular usage, refers to a subbasin of the Jordan Valley that extends between the Great Salt Lake and the Traverse Range, which is a range of hills to the south that runs transverse to the Jordan Valley and separates it from another subbasin farther south, the "Utah Lake Valley." The Jordan River cuts through the Traverse Range at the Jordan Narrows.

FIG. 1. Photograph of the low-angle slope looking west-northwest from the tower site.

The design of the slope-flow experiment took advantage of the presence of a near-ideal homogeneous slope on the western side of the Salt Lake Valley (Fig. 1). The slope owes its smooth surface and lack of major corrugations or tributaries to wave action on the ancient shoreline of glacial Lake Bonneville. The Great Salt Lake is the present-day remnant of this ice-age lake. Experiments were conducted on this smooth, uniform, low-angle (~1.6°) slope on the floor of the Salt Lake Valley at the foot of the Oquirrh Mountains 28 km south-southwest of Salt Lake City. The site was chosen for its uniform topographic and surface characteristics, its accessibility, and its altitude, which was within the normal height range of the nocturnal valley inversion, thus assuring regular diurnal changes in ambient stability over the slope. Because of low precipitation amounts, the slope is normally strip cropped and, during the October experiments, the slope had alternating strips of wheat stubble and disked soil. The azimuth, slope, and soil at the slope site are broadly representative of much of the western side of the Salt Lake Valley below the steeper slopes of the Oquirrh Mountains. A huge open-pit copper mine (Kennecott Utah Copper's Bingham Canyon mine) and its Bingham Canyon drainage channel to the west of the site (Fig. 2) were expected to intercept downslope flow from the higher terrain of the Oquirrh Mountains and channel it to the northwest of the slope site. The waste-rock pile on the east side of the open-pit mine was, nonetheless, uphill from the slope site. The effect of downslope flows from this slope on the katabatic flows that develop on the low-angle slope at its base is an important research question that will be discussed further in this paper and in Part II.

The meteorological equipment and locations are listed in Table 1 and are shown in Figs. 2 and 3. Figure 2 shows the experimental area and the instrument locations. The Salt Lake Valley or Jordan Valley drains northward and northwestward into the Great Salt Lake. Figure 3 shows further topographic detail and instrument locations in the vicinity of the slope experiment site. A comparison of contours at the slope site with those at higher altitudes illustrates the strong influence of wave action in smoothing the slope contours at the experiment site. Figure 4 is a topographic cross section from the ridgeline of Bingham Canyon northwest of (and up the terrain gradient from) the uppermost tethered-balloon site down the slope through the remaining three tethersonde ("sonde") sites. The uppermost tethersonde site was approximately 3.5 km east of the base of the waste-rock pile shown in Fig. 2. The tethersonde sites TS1, TS2, TS3, and TS4 were numbered from the lowest to the highest altitudes—1485, 1513, 1539, and 1572 m MSL, respectively. Frequent soundings were made concurrently with all of the tethered balloons to heights of 200–300 m. Occasional deeper ascents to approximately 450 m were made at TS1 to sample the valley atmosphere above the slope boundary layer. After the ascents, balloons were retrieved quickly and were allowed to equilibrate at the ground before their next ascents. Down-soundings were discarded and have not been used in the analyses. The sondes measured temperature, relative humidity, pressure, wind speed, and wind direction. Pre- and postexperiment calibrations were performed, and the data were corrected for the minor differences noted.

Additional supporting instruments whose locations are shown in Figs. 2 and 3 include automatic weather stations WS1 and WS2 near TS1 and TS4 and a scanning water vapor lidar between TS3 and TS4 (Cooper et al. 2006). Gasoline-powered generators were used for power at the tethersonde sites, and batteries and

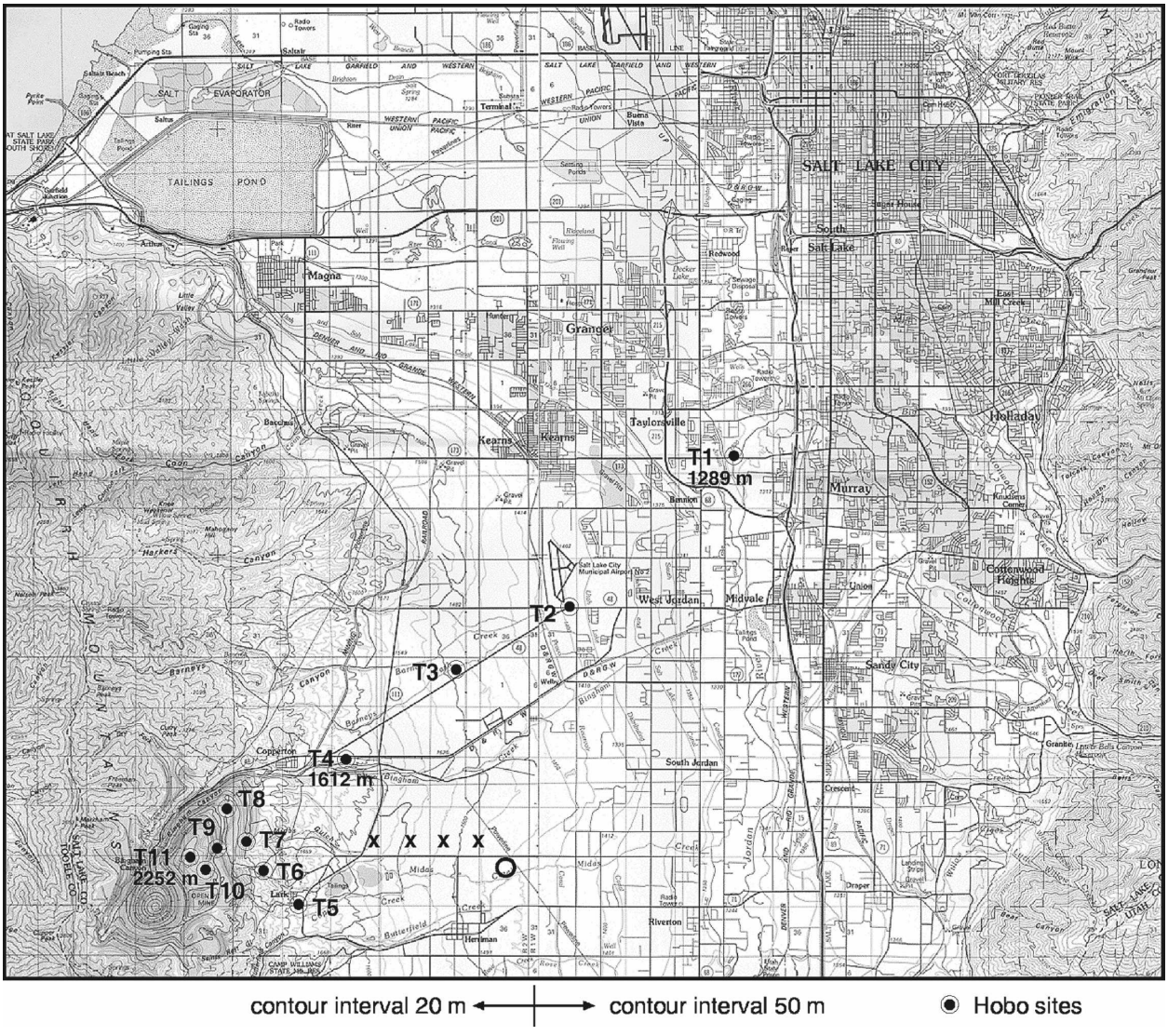

FIG. 2. Map of the Salt Lake Valley or subbasin. Shown are the locations of temperature dataloggers T1–T11 (black dots), tethered balloon sounding systems (x), and a meteorological tower (circle). The southern end of the Great Salt Lake (1280 m MSL) is shown in the upper left, and the Salt Lake City urban center is at the upper right. The ridgeline of the Oquirrh Mountains is on the left of the figure, and the ridgeline of the north–south-oriented Wasatch Mountains is off the figure to the right. The circular contours southwest of T11 are the open-pit mine. Sites T7–T11 are on the waste-rock pile. Note the north–south boundary that marks the change in contour interval from 20 to 50 m where the two maps are spliced together. The base map is from the U.S. Geological Survey 1:100 000 Tooele, UT, and Salt Lake City quadrangles.

solar panels were used at the automatic weather stations. A site on the slope 1.35 km southeast of TS1 had line power that was used for a sonic anemometer at the 9.1-m level of a tower, two thermocouples at the 1- and 3-m levels of the tower, a scintillometer, and a Doppler minisodar. In addition, a line of 11 battery-operated Hobo Pro temperature dataloggers (manufactured by Onset Computer of Bourne, Massachusetts) in self-aspirated radiation shields ran up the western sidewall of the valley from the Jordan River to the top of the waste-rock pile with a vertical spacing of approximately 100 m. These loggers collected data at 5-min intervals. Laboratory and field tests of these dataloggers were reported by Whiteman et al. (2000).

b. The dataset

Data were collected continuously from the weather stations and thermocouples during the entire VTMX experimental period from 1 to 27 October. The minisodar, scintillometer, and sonic anemometer were shut

TABLE 1. Instrument locations.

Site	Lon (°W)	Lat (°N)	Elev (m MSL)	Comments
Tethersonde TS1	112.023 83	40.544 30	1485	
Tethersonde TS2	112.036 98	40.543 50	1513	
Tethersonde TS3	112.047 17	40.544 00	1539	
Tethersonde TS4	112.061 73	40.543 05	1572	
Lower weather station WS1	112.023 55	40.539 43	1485	
Upper weather station WS2	112.062 10	40.542 05	1572	
Tower 3D eddy correlation	112.013 10	40.536 45	1466 (base)	9.1 m AGL
Tower thermocouple	112.013 10	40.536 45	1466 (base)	1 m AGL
Tower thermocouple	112.013 10	40.536 45	1466 (base)	3 m AGL
Scintillometer transmitter	112.013 12	40.536 42	1466	
Scintillometer receiver	112.013 27	40.534 95	1468	
Minisodar	112.013 23	40.536 35	1467	
Radar profiler	112.065 43	40.544 27	1579	
Water vapor lidar L	112.058 35	40.543 27	1565	
Temperature logger T1	111.925 27	40.653 65	1289	1.73 m AGL
Temperature logger T2	111.987 43	40.609 70	1393	1.35 m AGL
Temperature logger T3	112.031 82	40.592 27	1481	1.29 m AGL
Temperature logger T4	112.074 85	40.565 70	1612	1.31 m AGL
Temperature logger T5	112.093 40	40.523 48	1682	1.25 m AGL
Temperature logger T6	112.107 00	40.533 42	1820	1.30 m AGL
Temperature logger T7	112.112 20	40.542 48	1878	1.32 m AGL
Temperature logger T8	112.120 28	40.552 62	1954	1.24 m AGL
Temperature logger T9	112.125 00	40.540 38	2051	1.18 m AGL
Temperature logger T10	112.127 32	40.534 10	2155	1.33 m AGL
Temperature logger T11	112.135 05	40.536 88	2252	1.34 m AGL

down only during a few rainy subperiods. However, 9 of the 11 temperature dataloggers that collected data for the year preceding the experiment failed after a hardware modification on 4 October. Tethersondes were operated (Table 2) during eight of the ten 21-h intensive observational periods (IOPs) that were declared by VTMX investigators on the basis of weather forecasts (Doran et al. 2002), collecting a total of 369 soundings. These eight IOPs began at 1500 mountain standard time (MST; MST = UTC − 7 h) on 2, 6, 7, 8, 14, 16, 19, and 25 October (IOPs 1–6, 8, and 10, respectively). Channeled winds in the valley were too strong to fly the tethered balloons at the slope site during IOPs 7 and 9. The IOPs were generally chosen to maximize the occurrence of drainage flows and the buildup of a stable atmosphere inside the Salt Lake Valley. Other VTMX participants conducted experiments on the east sidewall of the Salt Lake Valley and from the Great Salt Lake north of the valley to the Jordan Narrows to the south. A surprising finding (Doran et al. 2002) was that there were often large differences in local meteorological conditions from one side of the valley to another, affected primarily by large vertical axis eddies that formed in different parts of the valley and appeared to be driven by strong flows exiting from major tributaries on the east side of the valley, especially Parley's Canyon. At times, vastly different meteorological conditions occurred on the east and west sides of the valley. In IOP 2, for example, a shallow easterly downslope windstorm (Holland 2002) was in progress in the university district on the lower-east sidewall of the valley above the Salt Lake City urban center while relatively undisturbed drainage flows were present at our slope site.

Because large numbers of personnel were required to operate the four tethered balloon systems, the limited staffing generally required choices concerning during which hours to operate during the 21-h IOPs. Our observations were made mostly during the evenings, but tethersonde data were also collected during other times of day in some of the IOPs (see Table 2), including the late afternoon, the evening, the night, and the postsunrise slope-flow-reversal and inversion-breakup period. In this paper we discuss only periods of downslope-flow evolution. Thermally driven downslope flows were in evidence on the slope on all clear, undisturbed nights, but in this paper we illustrate downslope-flow evolution using tethered balloon ascents during two periods in which skies were clear, upper winds were weak, and downslope flows were well developed. The two periods include the evening period from 1800 to 2200 MST 2 October 2000 (IOP 1) and the evening and nighttime period of 8–9 October 2000 (IOP 4). For reference, astronomical sunrise and sunset occurred at 0628 and

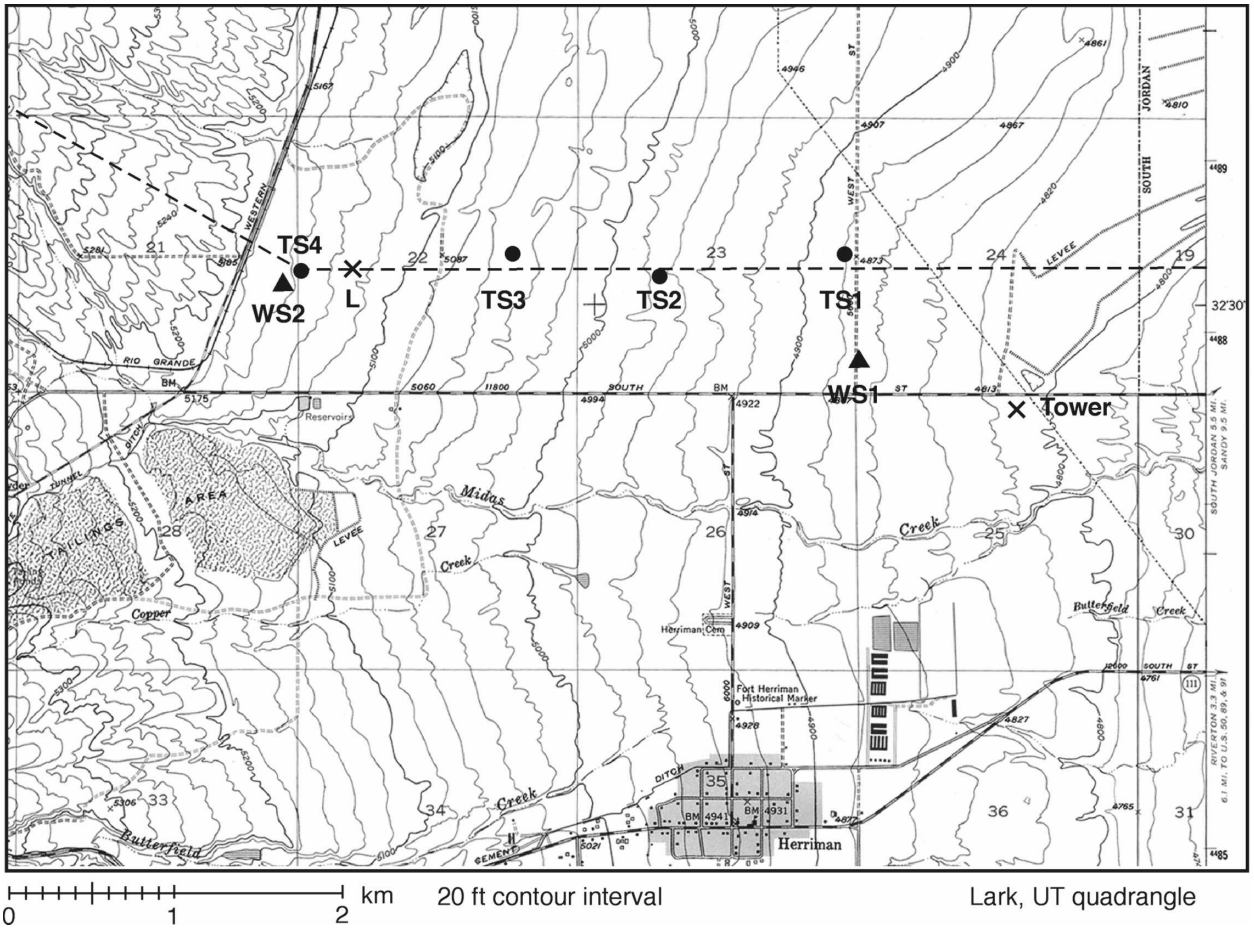

FIG. 3. Contour map of the slope area, showing the locations of the tethersondes TS1–TS4, automatic weather stations (WS1 and WS2), and water vapor lidar (L). A minisodar and a scintillometer were collocated at the tower site (X), which had an eddy correlation instrument at the 9.1-m level and thermocouples at the 1- and 3-m levels. The dashed line indicates the location of the topographic cross section of Fig. 4. The contour interval is 20 ft (6.1 m). The base map is from the U.S. Geological Survey 1:24 000 Lark, UT, quadrangle.

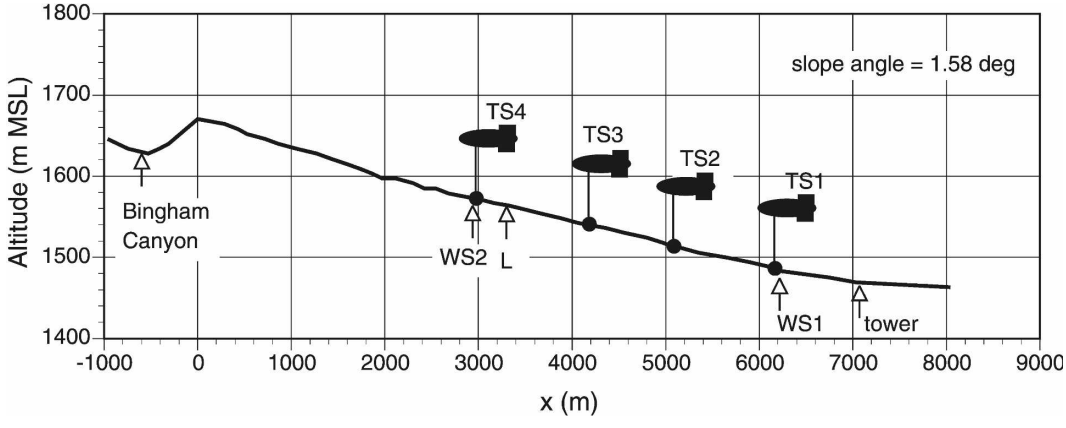

FIG. 4. Topographic cross section of the slope showing tethersonde sites TS1–TS4, automatic weather stations (WS1 and WS2), water vapor lidar (L), and the tower site where the sonic anemometer, scintillometer, thermocouples, and minisodar were located. The terrain cross section is drawn along the line indicated on Fig. 3, and the instruments located off this line have been projected northward or southward onto the cross section.

TABLE 2. Tethersonde data inventory.

IOP	October (day)	Sounding starting times (MST), number of soundings
1	2–3	TS1–3: 1806–2130, 8 soundings each TS4: 1723–1803, 2 soundings
2	6–7	TS1–3: 1745–2128, 7 soundings each TS4: 1659–1930, 3 soundings
3	7–8	All: 1722–1836, 3 soundings each
4	8–9	TS1–3: 1713–0527, 17 soundings each TS4: 1706–2135, nine soundings
5	14–15	TS1–3: 1722–0849, 21 soundings each TS4: 1713–2129, 11 soundings
6	16–17	TS1–3: 0351–0926, 18 soundings each TS4: 0358–0929, 11 soundings
8	19–20	TS1–3: 0341–0859, 13 soundings each TS4: 0330–1028, 14 soundings
10	25–26	All: 1731–2349, 14 soundings each

1807 MST on 2 October and at 0635 and 1758 MST 8 October. The first period had the best-developed evening downslope flows, but was at a time when much of the supporting instrumentation (e.g., minisodar, sonic anemometer) was not yet operational on the slope. During the second of these periods, all of the supporting equipment was operational and the observations were continued throughout the entire night. Both periods had low humidity and strong outgoing longwave radiation, so that nocturnal temperature inversions built up within the valley. On 2 October the observations were stopped before midnight, when a northerly synoptic-scale pressure gradient began to reverse the normal nocturnal down-valley flow in the valley. After 0500 MST 9 October an approaching trough caused southerly winds to intrude into the valley. Further information on the synoptic weather conditions during VTMX IOPs is available from Doran et al. (2002).

3. The structure and evolution of the observed downslope flows

As expected from valley-wind theory (Wagner 1938; Whiteman 1990, 2000), winds in the Salt Lake Valley during fair weather periods were normally up valley (i.e., from the north) during daytime and down valley (i.e., from the south) during nighttime, with transition periods in the morning and again in the late afternoon or early evening when the weakening along-valley winds allowed the up- and downslope winds to be most clearly expressed over the slopes. Often, after midnight, as the down-valley wind strengthened and a stronger background ambient stratification developed over the slope with the upward growth of a temperature inversion from the valley floor, the downslope flows decayed or became intermittent. Downslope winds, in addition to being sensitive to the influence of the normally down-valley flow above the slope, were also affected by larger-scale flows above the valley that were channeled along the valley's axis or were superimposed on the along-valley flows (e.g., Banta et al. 2004). Because the downslope and down-valley winds, as in most valleys, were typically in orthogonal directions, there was often considerable directional shear through the slope-flow layer. Examples of these features are selected from IOPs 1 and 4.

a. IOP 4: The downslope-flow period with the best supporting data

A time–height cross section of hour-average vector winds for IOP4 from the minisodar is shown in Fig. 5. These data have 5-m range resolution, the lowest data are at 15 m AGL, and the hourly vector averages shown were obtained from the original 5-min averages. The solid lines in the figure qualitatively partition the wind data into time–height areas containing primarily up-valley (northerly), downslope (westerly), down-valley (southerly), and channeled synoptic winds. The 1800 MST sounding had northerly up-valley winds throughout the profile, as expected from valley-wind theory, except at the lowest minisodar level where the wind had already begun to turn into the downslope direction. By 1900 MST, the downslope winds extended to depths of more than 100 m. The downslope wind subsequently developed over the slope to attain maximum speeds of 5–6 m s^{-1} by 2100–2200 MST, jet heights below 20 m AGL, and downslope-flow depths of 80–125 m. The strength and depth of the downslope flow layer decreased after 2100 MST as the up-valley winds above the downslope-flow layer shifted to down valley, strengthened, and extended closer to the ground. At around 0500 MST, southeasterly winds were first seen at the upper range gates of the minisodar. These channeled winds strengthened and descended into the valley as a trough approached from the west. These channeled synoptic winds overrode the normal daytime cycle of thermally driven flows, which call for upslope (i.e., easterly) flows after sunrise with a subsequent shifting of winds to up valley.

Consecutive tethered-balloon soundings of potential temperature and downslope and cross-slope wind velocity components are shown in Fig. 6 for IOP 4. For the winds, a Cartesian coordinate system is used in which a pure downslope wind (assumed from topographic maps to be from 273°) produces a positive u component and a wind from 183° produces a positive v component. The background potential temperature stratification for these soundings, determined from the

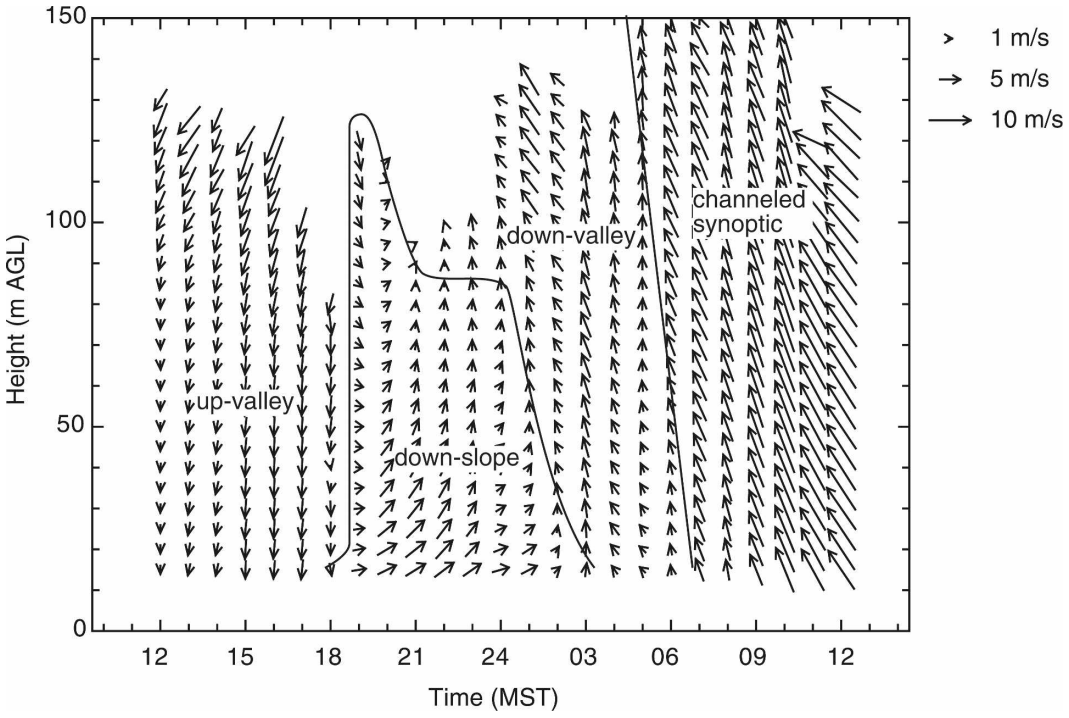

FIG. 5. Minisodar time–height cross section of horizontal wind vectors during IOP 4 on 8–9 Oct 2000. A vector pointing up indicates a south wind, a vector pointing to the right indicates a west wind, etc. Speeds are indicated by the vector length, as shown in the legend.

mean potential temperature gradient above the slope-flow layer in the tethersonde soundings, was 10 K km^{-1}. The first sounding, at 1714 MST, had a near-neutral potential temperature profile with upslope and cross-slope winds (i.e., up-valley winds) over all four slope sites. By the 1751 MST sounding, however, the sensible heat flux had reversed (Fig. 7), a shallow stable layer had formed above the slope sites, and downslope winds had been initiated in the lowest few meters above the surface, with upslope and up-valley winds remaining aloft. During the ensuing evening evolution of the slope flows, the sensible heat flux, as measured by a sonic anemometer at the 9.1 m AGL level from the tower site (Fig. 2) and by a scintillometer with a 100-m-long path and a mean height of 2.6 m above the slope, averaged only 10–15 W m^{-2}, with increasing intermittency and sign changes after late evening. By 1819 MST (Fig. 6), the flows had grown to about 30 m AGL, with a layer of upslope flows still remaining above them. By 1857 MST, the downslope-flow layer was more than 100 m deep, with maximum wind speeds reaching 4–5 m s^{-1} approximately 10 m above the slope, and with the maximum speeds increasing with distance down the slope from TS4 to TS3 to TS2. The wind speed maxima were approximately equal at TS2 and TS1. The jet speed profile was very sharp at the lowest three sites but had a more rounded appearance at TS4. Sharp potential temperature inversions had developed over the slope sites (Fig. 6), with potential temperatures increasing by 5–7 K over a 10–15-m-deep layer. The convergence of the potential temperature profiles (and, to a lesser extent, the wind profiles) above the shallow stable layer indicates that the atmospheric structure was approximately horizontally homogeneous above this shallow layer. By 1819 MST the up-valley winds above the slope-flow layer had begun to decrease in strength, and by 1857 MST the winds had reversed to down valley. Winds maintained this down-valley direction for the rest of the night. An increase in the speed of the downslope jet maximum with downslope distance is clearly seen in the 1857 and 2028 MST soundings. This suggests that downslope mass flux increases with downslope distance—a question that will be investigated further in section 6. By the 2101 MST sounding (not shown), the depth of the downslope flows had decreased at all sites as the down-valley flow aloft became stronger. This is also apparent in the 2217 MST sounding. Downslope flows became shallower, weaker, and more nonstationary after about 2100 MST, despite only weak changes in the structure and intensity of the shallow high-stability layer just above the slopes. This nonstationarity occurred at a time when vertical

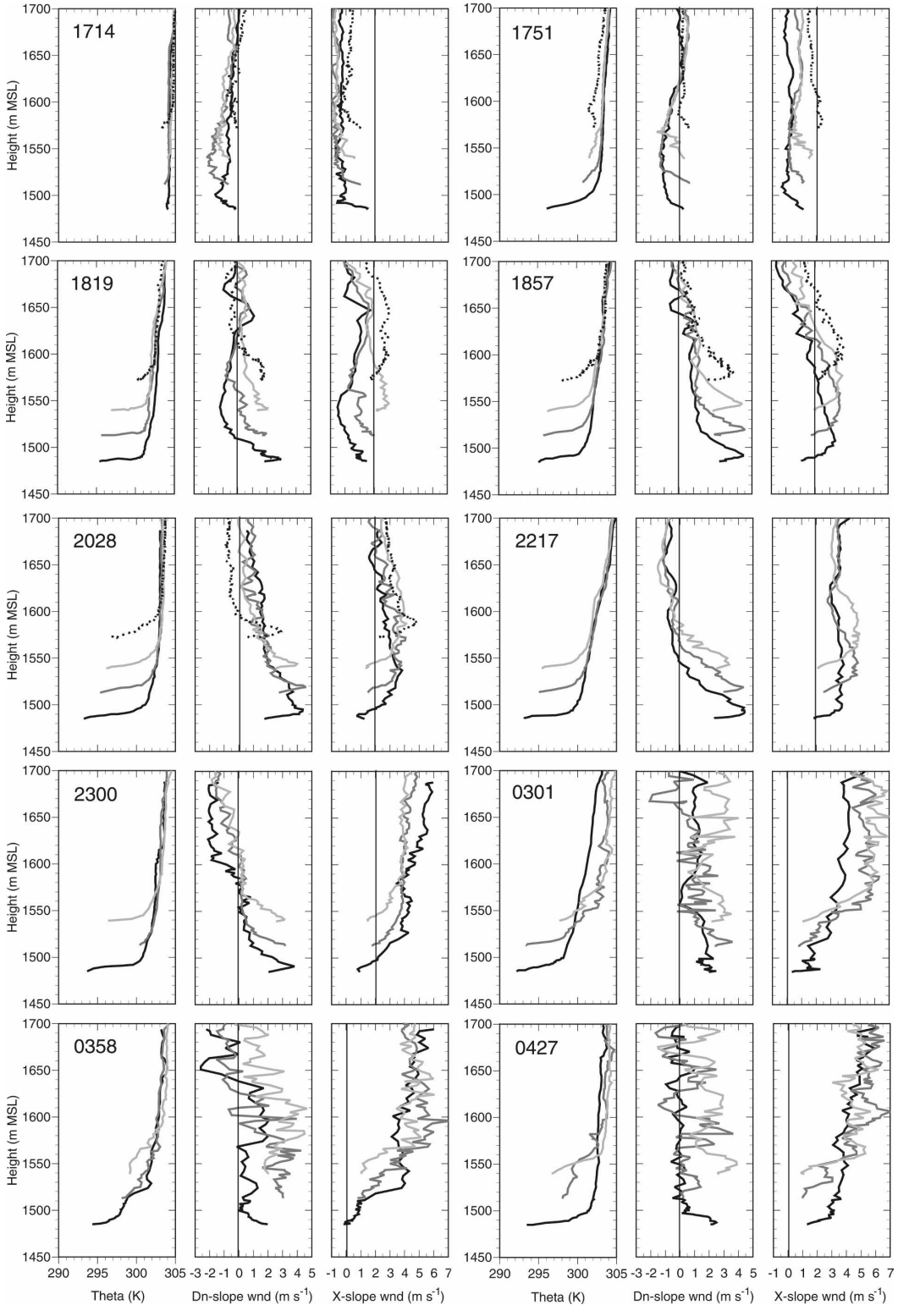

FIG. 6. Selected soundings of potential temperature (theta; K), downslope wind speed component (m s^{-1}), and cross-slope wind speed component (m s^{-1}) during IOP 4 on 8–9 Oct 2000 from the four tethersonde sites TS1 (black), TS2 (dark gray), TS3 (light gray), and TS4 (dashed black) at the times (MST) indicated. The abscissas on the downslope wind component subfigures run from −3 to +5 m s^{-1}. The abscissas on the cross-slope panels run from −3 to +5 m s^{-1} for all but the last three panels, for which they run from −1 to +7 m s^{-1}.

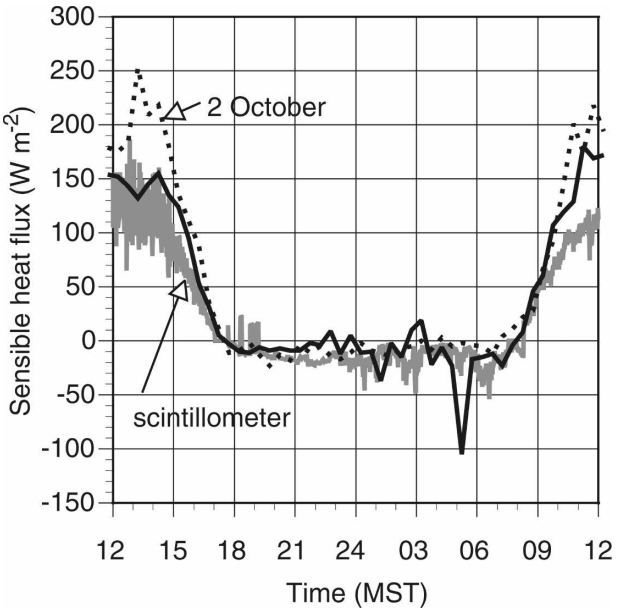

FIG. 7. Sensible heat flux during IOP 4 on 8–9 Oct 2000 as measured by a sonic anemometer at 9.1 m AGL (solid line) and a scintillometer with mean height of 2.6 m AGL (gray line). For comparison, the dashed line shows sonic anemometer data from 2 Oct 2000.

potential temperature gradients above the shallow inversion layers (i.e., "ambient stability") became somewhat more variable than was observed in the early-evening (1819–2028 MST) soundings. Potential temperature soundings before 0301 MST at the slope sites were nearly coincident above the shallow stable layer, whereas later soundings show increasingly large horizontal changes in potential temperature between sites at a time when the shallow, strong-stability layers above the slopes began to decay and the downslope flows became weak and intermittent.

b. *IOP 1: The downslope-flow period with the best-developed flows*

The best downslope flows were observed in the evening of 2 October 2000. Downslope wind speed component and potential temperature profiles for this evening are shown from tethersonde soundings in Fig. 8. However, TS4 soundings were available only in the early evening on this date. The background potential temperature stratification for this evening was 2.5 K km^{-1}. At 1757 MST, downslope winds were weak (generally < 2 m s^{-1}) at all altitudes and sites. By 1836, katabatic jet profiles had developed above the slope at all sites, with the strongest maximum speed of 5 m s^{-1} at the lowest site and the weakest maximum speed of 4 m s^{-1} at the highest-altitude site. Through the rest of the evening the slope flows fluctuated somewhat in speed from time to time but generally attained depths of about 150 m AGL with maximum speeds of 4–7 m s^{-1} at about 15 m AGL. At 1757 MST, shallow potential temperature deficits were already present above each of the slope sites, with the maximum deficit of 5 K at the surface at TS3. By 1836 MST the slope temperature deficits extended to 25–50 m AGL and strengthened to 6–8 K. The coldest surface temperatures occurred at the lowest-elevation sites. The potential temperature deficits strengthened slightly as the evening progressed, approaching 8 K. The potential temperature deficits were confined mostly to the lowest 50 m, and the deficits decreased slightly with upslope distance. The katabatic flow began to decay by the 2121 MST sounding, perhaps because of a buildup in ambient stability in the valley below. The earlier soundings exhibited mean katabatic flow depths of about 150 m at the two sites that were farthest downslope. The mean flow was about 10% deeper at the uppermost site. The potential temperature deficit as averaged over the full flow depth varied from site to site, with TS2 often being a pivot point, so that the mean temperature deficits were larger or smaller at the adjacent sites. The downslope volume flux increased with downslope distance.

Automatic weather station data at site WS1 (location shown in Fig. 3) show how the winds on the slope behaved throughout the night (Fig. 9). During the evening period of downslope flows, winds were from the west at speeds of 3 m s^{-1} at the anemometer height of 3 m. At approximately 2300 MST, as the along-slope temperature boundary layer became more isothermal and as incoherent oscillations began to occur at all of the temperature-datalogger sites, the downslope wind began to decay, with large oscillations in direction and decreases in speed. Winds became steady again in the downslope direction at 0130 MST, but the wind speeds during the remainder of the night reached only 1.5–2.3 m s^{-1}.

4. Effects of ambient stability

The effect of ambient stability on the katabatic-flow development is revealed by comparing the tethered-balloon soundings from IOP 1 (Fig. 8) with those from IOP 4 (Fig. 6). As indicated by a larger vertical potential temperature gradient immediately above the inversion layer, the ambient atmosphere was more stable on the evening of 8 October during IOP 4 than on 2 October in IOP 1. The stronger stability of the ambient environment was also evident in the comparison of radiosonde soundings launched at Wheeler Farm, the main VTMX sounding site to the northeast of the slope site over the floor of the valley, during the two evenings (not shown). Although small differences existed among the various soundings taken at different times during

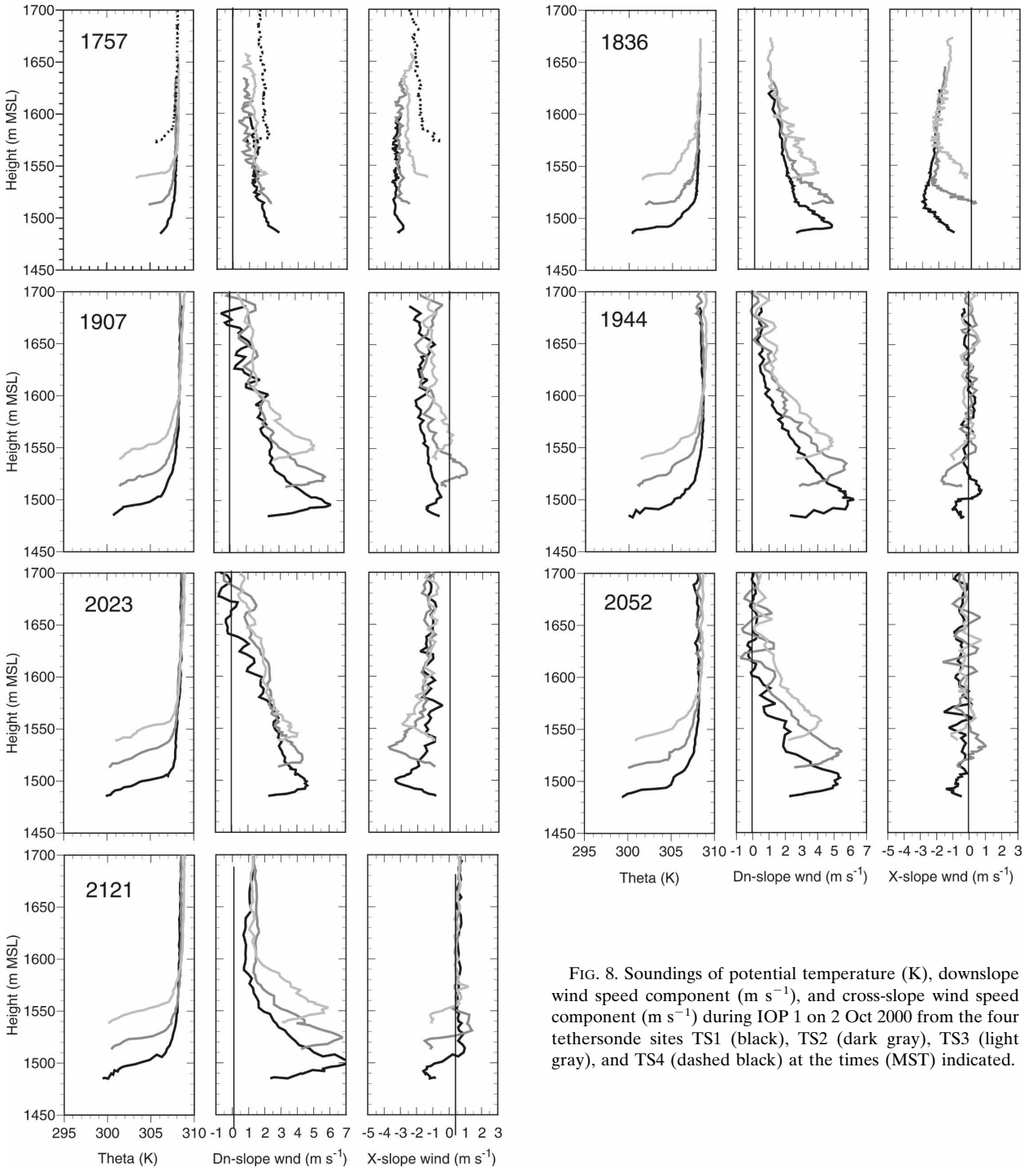

FIG. 8. Soundings of potential temperature (K), downslope wind speed component (m s^{-1}), and cross-slope wind speed component (m s^{-1}) during IOP 1 on 2 Oct 2000 from the four tethersonde sites TS1 (black), TS2 (dark gray), TS3 (light gray), and TS4 (dashed black) at the times (MST) indicated.

both evenings, the rates of increase in potential temperatures in the lowest 1 km of the atmosphere from the top of the inversion was generally 1°–2°C km^{-1} on 2 October, and they more than tripled on 8 October to 5°–8°C km^{-1}.

Stronger ambient stability on the evening of 8 October resulted in weaker katabatic flows. The peak jet speed ranged between 4 and 5 m s^{-1} during this evening as compared with 5–7 m s^{-1} on 2 October, when the ambient environment was near neutral. The heights of the wind maxima and the depths of the katabatic flow, however, appeared to be less sensitive to ambient stability, because they remained similar on both evenings.

An evaluation of the effects of atmospheric stability

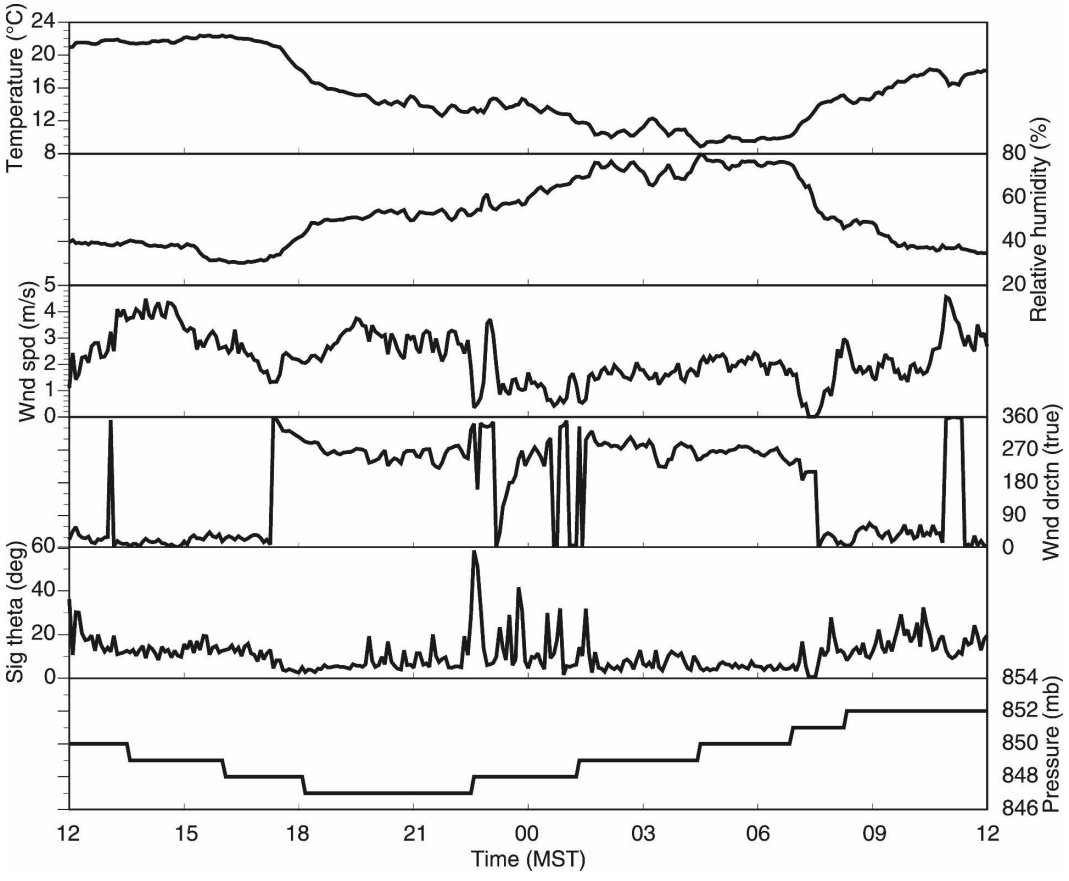

FIG. 9. Time series of temperature, relative humidity, wind speed, wind direction, standard deviation of wind direction, and atmospheric pressure from WS1 during IOP 1 on 2–3 Oct 2000.

on slope-flow development was attempted for other experimental nights using radio acoustic sounding system and rawinsonde data. These evaluations were, however, inconclusive because of the wide variation in ambient or background winds, which act in conjunction with atmospheric stability to affect slope flow development. Our approach to determining the separate effects of stability and ambient wind was then shifted to using a parametric study with a suitable numerical flow model. The model results are reported in Part II.

5. Sensitivity to ambient winds

Downslope flows are sensitive to the ambient winds that develop above them. During the evening in the lowest few meters above the slope, downslope winds blew directly down the topographic gradient of the slope. With altitude, however, the wind shifted progressively into the direction of the ambient flow above the slope-flow layer, typically attaining the ambient flow direction at the top of the temperature deficit layer about 25 m above the slope. This is seen for selected soundings from IOP 1 in Fig. 10 (e.g., the 1836 MST sounding). Above this level, the ambient-flow direction was generally constant with height and did not vary significantly from site to site on constant MSL height surfaces, that is, in the cross-valley direction above the slope-flow layer. The ambient-wind direction above the slope in the late afternoon and early evening before a strong down-valley flow began varied from IOP to IOP, depending on the synoptic wind direction and the degree to which this was channeled into the valley.

During the course of an evening, the winds above the slope flow layer typically turned down valley and increased in strength. This usually occurred late in the evening, as seen in Fig. 6 for IOP 4, when the cross-valley wind components began to increase by the 2217 MST sounding. The down-valley wind often appeared in the form of a nocturnal down-valley jet that came northward into the Salt Lake Valley from the Utah Lake Valley over the Traverse Range (Banta et al. 2004).

The fact that the wind turning occurs in such close proximity to the slope and turns continuously through the jet maximum where the wind shear goes through a

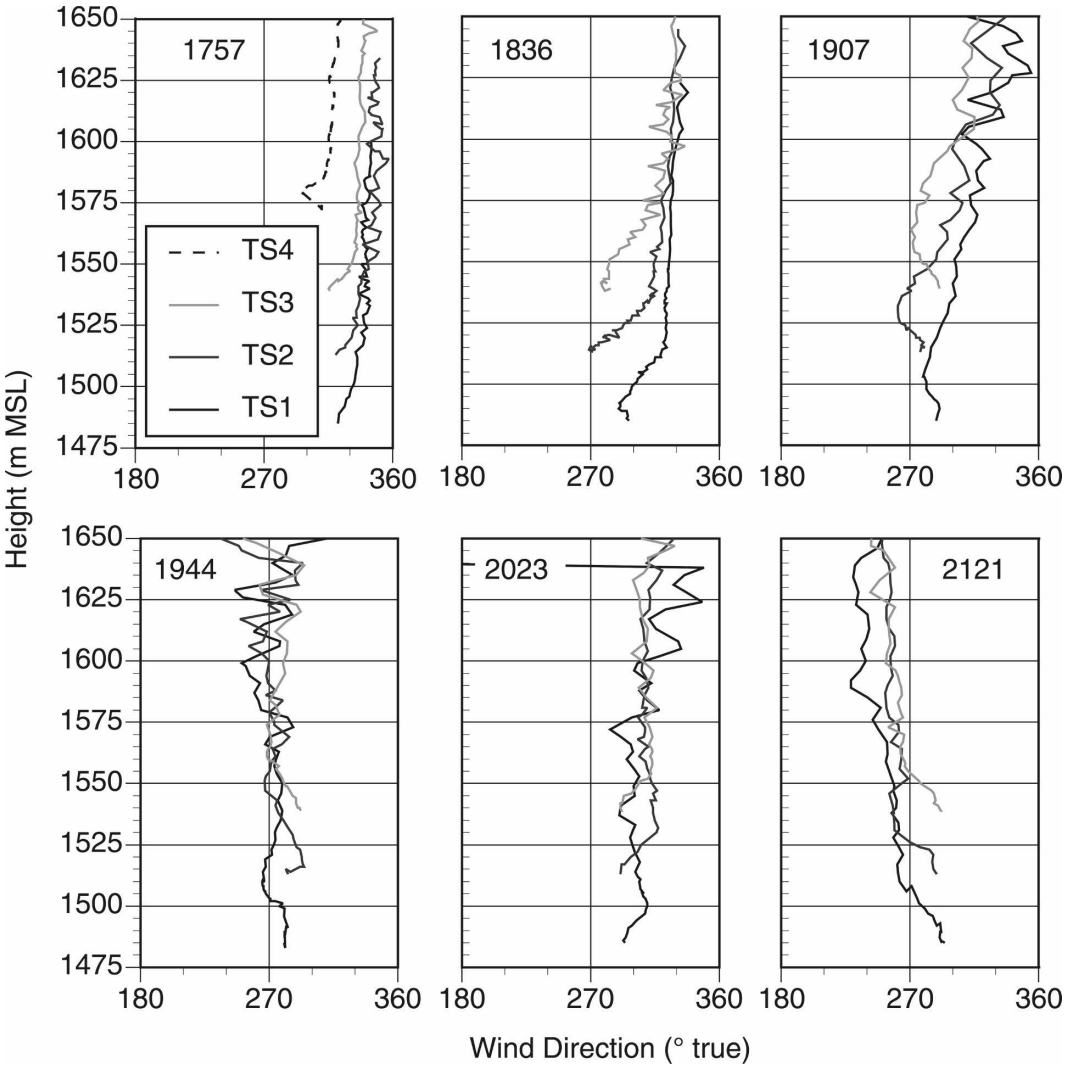

FIG. 10. Wind direction soundings during the times of strongest downslope flows during IOP 1 on 2 Oct 2000.

local zero (speed shear is positive below and negative above the height of the jet maximum) is a somewhat unexpected result that causes the jet speed maximum to blow at an angle relative to the local downslope topography gradient. This characteristic of the slope flow makes prediction of dispersion on slopes difficult, because a strong directional shear in a shallow layer above the slope would cause plumes that are released at slightly different heights to travel in very different directions. Winds may either back or veer with height to reach the ambient flow direction, generally turning through the smallest angle required to reach the ambient wind direction.

6. Discussion

The variation with downslope distance of key properties of the downslope-flow layer can be summarized from the detailed tethersonde soundings at the individual sites. This is done in Fig. 11 for 2 October 2000 (IOP 1), the night on which the downslope flows were best developed. Figure 11 uses downslope-flow depths and potential temperature deficits analyzed from the soundings in Fig. 8. The variation of the depth of the downslope-flow layer with downslope distance is shown in Fig. 11a. Downslope-flow-layer depths were generally in the range from 140 to 200 m AGL at all sites and times, except for the last sounding, for which depths had decreased at TS1 and TS2 to values of 80 and 102 m, respectively. In general, there was little variation in downslope-flow depth with downslope distance. The mean potential temperature deficits are given in Fig. 11b. The slope potential temperature deficit generally extended to heights of about 25 m above the slope sites. The deficits show much variability from site to site and

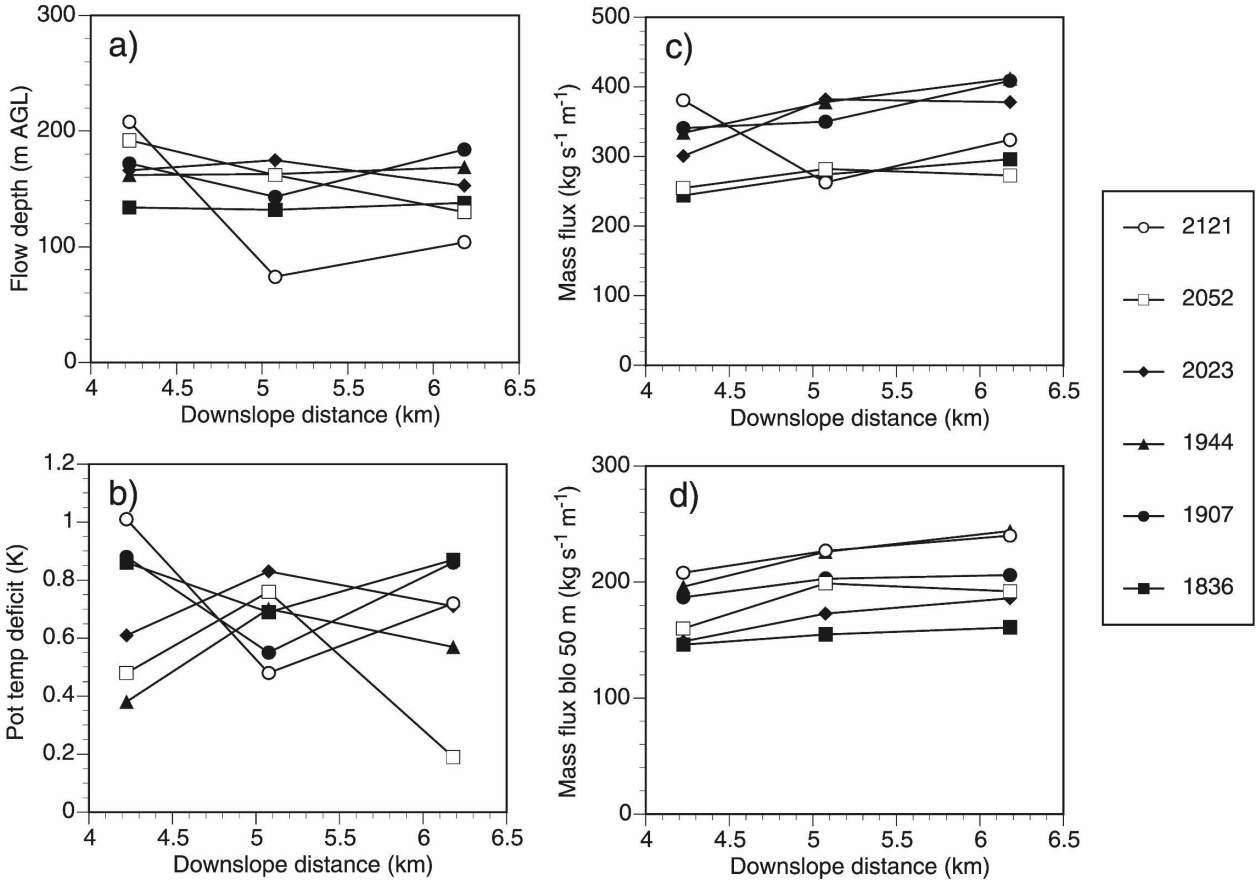

FIG. 11. (a) Katabatic flow depth, (b) potential temperature deficit, (c) total downslope mass flux, and (d) downslope mass flux to a height of 50 m AGL (kg s^{-1} m^{-1}) are shown as a function of downslope distance at the times indicated in the legend (MST) during IOP 1 on 2 Oct 2000. Symbols are plotted at downslope distances corresponding to TS3 (4.2 km below the eastern edge of Bingham Canyon on the cross section of Fig. 4), TS2, and TS1, respectively.

from time to time, with the middle tethersonde deficits being sometimes larger and sometimes smaller than the potential temperature deficits at the adjacent uphill and downhill sites. Mean downslope mass fluxes through the depth of the downslope-flow layer (Fig. 11c) and through the lowest 50 m (Fig. 11d) increase with distance downslope and are on the order of 300 and 200 kg s^{-1} m^{-1}, respectively. These increases in mass flux are driven primarily by an increase in drainage-flow speed with downslope distance. Because atmospheric density at the altitude of the slope site is approximately 1 kg m^{-3}, volume fluxes would have similar numerical values. If the downslope flows at this site are representative of other locations along the base of the Oquirrh Mountains on the west side of the Salt Lake Valley, the downslope mass flux at this altitude along the approximately 20-km-long base of the Oquirrh Mountains would be approximately 6000 t s^{-1}. This would correspond to a volume flux of 22 km^3 h^{-1}. It would be interesting, in future work, to compare these mass fluxes on the west sidewall of the Salt Lake Valley with mass fluxes over the east sidewall of the valley, including the mass fluxes issuing from the major east sidewall tributaries (e.g., Parley's Canyon and Big and Little Cottonwood Canyons).

The similar shapes of the downslope wind profiles and their near-simultaneous development at different sites suggests that the flow is driven by local forcing. It is not clear, however, whether the profiles are influenced by stronger flows coming from steeper topography farther up the slope. This question is addressed further by model simulations in Part II.

7. Conclusions

Downslope or drainage flows on a very low angle (~1.6°) slope in the Salt Lake Valley were deeper and stronger than have been reported previously by other investigators (e.g., Manins and Sawford 1979; Clements and Nappo 1983; Horst and Doran 1986), who generally

investigated steeper slopes and, in many cases, slopes on the sidewalls of isolated mountains where the nighttime buildup of ambient stability over the valley floor was not a complicating factor. Downslope flows in the Salt Lake Valley reached depths of 150 m AGL and strengths of 5–6 m s^{-1} at the 15-m height of the jet maximum. The temperature deficit over the slope reached 7°C at 25 m AGL, which is a comparable or slightly higher deficit than that reported by others. The downslope flows began at approximately the same time over the instrumented length of the slope and were initiated as the slope went into shadow just before astronomical sunset when the surface sensible heat flux changed sign. The downslope flow evolved mostly uniformly in time, rather than, for example, appearing as a sudden wind pulse shortly after sunset. Both the temperature deficit above the slope and the downslope flow strengthened with time in the early evening. The downslope flows weakened and became intermittent late in the evening (around midnight) as the down-valley flow strengthened and downward momentum transport turned the slope flow into the down-valley direction and suppressed its strength and depth.

The downslope flows appeared to be in local equilibrium, with the same wind and potential temperature profile shapes at all sites and with a regular development with downslope distance. There was some variation from night to night in the downslope development of the wind and temperature structure. The temperature deficit above the slope, the strength of the downslope jet, and its height above the ground generally increased with downslope distance. At given times, the wind speed increase from site to site with downslope distance was seen not only at the height of the jet maximum, but through the entire depth of the downslope flow.

The downslope flows in early evening produce substantial downslope mass or volume fluxes, estimated as 6000 t s^{-1} or 22 km^3 h^{-1} over the western side of the Salt Lake Valley. Most of this mass flux is carried in the lowest 50 m.

Analyses showed that the slope flows that were well developed in the early evening often became weak and intermittent in the middle of the night as a valley inversion built up to the altitude of the slope sites and as the overriding down-valley flow increased in strength and expanded to fill more of the valley cross section. Because the down-valley flow (or, any channeled flows within the valley) is at right angles to the underlying downslope flow, a significant directional shear occurs in the slope flow through heights that roughly coincide with the depth of the temperature deficit layer.

The slope-flow experiment demonstrated a new approach to observing downslope flows with a line of tethered balloons that was first tested in a smaller-scale experiment described by Clements et al. (2003). The commercial tethersonde system used in this experiment is normally purchased as a "tethersonde tower," in which multiple sondes are attached at different heights to a single balloonborne tether line that is left in place for some hours, producing time series measurements similar to those that would be obtained from fixed heights on a tall tower. A ground-based receiver cycles from sonde to sonde (the sondes transmit at different frequencies) to obtain time series data at the fixed sonde altitudes. In the slope-flow experiment, in contrast, the sondes were flown on separate balloons that were spaced about 1 km apart. The balloons were flown from separate winches in coordinated continuous ascents, with the data received and archived at a single ground-based receiver that cycled between the sondes. This system has the advantage of portability and of being able to produce the deep profiles necessary to observe downslope flows that exceed 150 m in depth without the expense of installing high towers. The disadvantage is that the ascents are "snapshots" of the slope flows, and there is no possibility of averaging the data or investigating high-frequency flow oscillations at fixed elevations.

Acknowledgments. Other VTMX investigators are thanked for providing their processed data. Al Astling and Fred Banes at the U.S. Army's Dugway Proving Ground provided and operated a tethersonde, a weather station, and a radar wind profiler. Rich Coulter at Argonne National Laboratory installed and operated the minisodar and scintillometer, Chris Doran at Pacific Northwest National Laboratory (PNNL) installed a tower and operated the sonic anemometer, and Dan Cooper of Los Alamos National Laboratory operated a scanning water vapor lidar. Tethersonde flights were conducted by Roland Mayr, Johanna Whiteman, Xindi Bian, Robert Grandy, James Stalker, Thomas Haiden, and Greg Poulos, with assistance from students from the Department of Meteorology at the University of Utah. Jerry Allwine, Chris Doran, Will Shaw, and John Hubbe from PNNL and Stephan de Wekker from the University of British Columbia helped to install equipment on the slope. Kennecott Utah Copper (Larry Trimble and Steve Schnoor) and their leaseholder, Dave Bastian, provided site permissions and assistance. Matt Krmpotich from Williams Gas Pipeline West and John Hayes from the South Valley Water Reclamation District also provided site access and power. The research was partially supported at PNNL by the U.S. Department of Energy (DOE) under the auspices of

the Atmospheric Science Program of the Office of Biological and Environmental Research and was partially supported by National Science Foundation Grants ATM-0521776 (CDW) and ATM-0646206 and ATM-0444807 (SZ). PNNL is operated for DOE by Battelle Memorial Institute.

REFERENCES

Allwine, K. J., J. H. Shinn, G. E. Streit, K. L. Clawson, and M. Brown, 2002: Overview of Urban 2000: A multiscale field study of dispersion through an urban environment. *Bull. Amer. Meteor. Soc.,* **83,** 521–536.

Banta, R. M., L. S. Darby, J. D. Fast, J. Pinto, C. D. Whiteman, W. J. Shaw, and B. D. Orr, 2004: Nocturnal low-level jet in a mountain basin complex. I: Evolution and effects on local flows. *J. Appl. Meteor.,* **43,** 1348–1365.

Briggs, G. A., 1979: Analytic modeling of drainage flows. NOAA/Atmospheric Turbulence and Diffusion Laboratory Contribution File No. 79/22, 15 pp.

Clements, C. B., C. D. Whiteman, and J. D. Horel, 2003: Cold-air-pool structure and evolution in a mountain basin: Peter Sinks, Utah. *J. Appl. Meteor.,* **42,** 752–768.

Clements, W. E., and C. J. Nappo, 1983: Observations of a drainage flow event on a high-altitude simple slope. *J. Climate Appl. Meteor.,* **22,** 331–335.

Cooper, D. I., M. Y. Leclerc, J. Archuleta, R. Coulter, W. E. Eichinger, C. Y. J. Kao, and C. J. Nappo, 2006: Mass exchange in the stable boundary layer by coherent structures. *Agric. For. Meteor.,* **136,** 114–131.

Coulter, R. L., M. S. Pekour, and T. J. Martin, 2004: Elevated stratified layers observed with sodar during VTMX. *J. Meteor. Atmos. Phys.,* **85,** 115–123.

Doran, J. C., 2004: Characteristics of intermittent turbulent temperature fluxes in stable conditions. *Bound.-Layer Meteor.,* **112,** 241–255.

——, J. D. Fast, and J. Horel, 2002: The VTMX 2000 campaign. *Bull. Amer. Meteor. Soc.,* **83,** 537–551.

Fast, J. D., K. J. Allwine, R. N. Dietz, K. L. Clawson, and J. C. Torcolini, 2006: Dispersion of perfluorocarbon tracers within the Salt Lake Valley during VTMX 2000. *J. Appl. Meteor. Climatol.,* **45,** 793–812.

Haiden, T., and C. D. Whiteman, 2005: Katabatic flow mechanisms on a low-angle slope. *J. Appl. Meteor.,* **44,** 113–126.

Holland, L., 2002: Downslope winds along the Wasatch Front. M.S. thesis, Department of Meteorology, University of Utah, 85 pp.

Horst, T. W., and J. C. Doran, 1986: Nocturnal drainage flow on simple slopes. *Bound.-Layer Meteor.,* **34,** 263–286.

Manins, P. C., and B. L. Sawford, 1979: Katabatic winds: A field case study. *Quart. J. Roy. Meteor. Soc.,* **105,** 1011–1025.

Monti, P., H. J. S. Fernando, M. Princevac, W. C. Chan, T. A. Kowalewski, and E. R. Pardyjak, 2002: Observations of flow and turbulence in the nocturnal boundary layer over a slope. *J. Atmos. Sci.,* **59,** 2513–2534.

Pinto, J. O., D. B. Parsons, W. O. J. Brown, S. Cohn, N. Chamberlain, and B. Morley, 2006: Coevolution of down-valley flow and the nocturnal boundary layer in complex terrain. *J. Appl. Meteor. Climatol.,* **45,** 1429–1449.

Poulos, G. S., 1997: The interaction of katabatic winds and mountain waves. Los Alamos National Laboratory Thesis (Ph.D.) LA-13224-T, 299 pp.

Skyllingstad, E. D., 2003: Large-eddy simulation of katabatic flows. *Bound.-Layer Meteor.,* **106,** 217–243.

Smith, C., and E. D. Skyllingstad, 2005: Numerical simulation of katabatic flow with changing slope angle. *Mon. Wea. Rev.,* **133,** 3065–3080.

Wagner, A., 1938: Theorie und Beobachtung der periodischen Gebirgswinde (Theory and observation of periodic mountain winds). *Ger. Beitr. Geophys.,* **52,** 408–449. [English translation: Whiteman, C. D., and E. Dreiseitl, 1984: Alpine meteorology: Translations of classic contributions by A. Wagner, E. Ekhart and F. Defant. Pacific Northwest Laboratory PNL-5141/ASCOT-84-3, 121 pp].

Whiteman, C. D., 1990: Observations of thermally developed wind systems in mountainous terrain. *Atmospheric Processes over Complex Terrain, Meteor. Monogr.,* No. 45, Amer. Meteor. Soc., 5–42.

——, 2000: *Mountain Meteorology: Fundamentals and Applications*. Oxford University Press, 355 pp.

——, J. M. Hubbe, and W. J. Shaw, 2000: Evaluation of an inexpensive temperature data logger for meteorological applications. *J. Atmos. Oceanic Technol.,* **17,** 77–81.

Zhong, S., and C. D. Whiteman, 2008: Downslope flows on a low-angle slope and their interactions with valley inversions. Part II: Numerical modeling. *J. Appl. Meteor. Climatol.*, **47,** 2039–2057.